Published on 19 August 2015. Downloaded by Huazhong University of Science & Technology on 23/11/2015 02:29:49.

RSC Advances

ROYAL SOCIETY OF CHEMISTRY

PAPER

View Article Online
View Journal | View Issue

Cite this: *RSC Adv.*, 2015, **5**, 71816

Tuning the morphology and composition of ultrathin cobalt oxide films *via* atomic layer deposition†

Bin Huang,‡[ab] Kun Cao,‡[ab] Xiao Liu,[ab] Lihua Qian,[c] Bin Shan*[b] and Rong Chen*[a]

Received 25th May 2015
Accepted 18th August 2015

DOI: 10.1039/c5ra09782g

www.rsc.org/advances

Ultrathin cobalt oxide (CoO_x) films (<10 nm) have been prepared on both planar and three dimensional substrates by atomic layer deposition (ALD) using $Co(Cp)_2$ and O_3 as precursors. The optimal temperature window was 150–250 °C with a saturated growth rate of ~0.37 Å per cycle. While the main composition of the thicker film consists of Co_3O_4 as verified by Raman spectroscopy, the initial few layers grown by ALD show a mixture of Co_3O_4 and CoO as revealed by X-ray photoelectron spectrum (XPS). The surface morphology of the film is greatly influenced by the deposition temperature as atomic force microscopy (AFM) and high-resolution transmission electron microscopy (HR-TEM) characterization show the formation of crystalline islands and uneven coating on porous structures at high temperatures, while a smooth and uniform coating can be obtained at lower temperatures. The role of nucleation sites and crystallization speed on film morphology is discussed. Furthermore, we show that tuning of deposition temperatures could lead to improved catalytic activities as demonstrated in the CO oxidation light off test.

1. Introduction

Cobalt oxide (CoO_x) is well known for its unique magnetic, catalytic and optical properties.[1–3] It has been widely used in energy storage,[4,5] air pollution control[6–8] and water catalytic oxidation[9] applications. Especially, ultrathin CoO_x films have been reported to exhibit outstanding catalytic activities better than their bulk counter parts.[10–12] For instance, 3–4 nm thick CoO_x films coated on photoanodes were proved to be very suitable for photoelectrochemical (PEC) water splitting.[13] Ultrathin CoO_x film modified $BiVO_4$ also shows improved PEC performance with enhanced stability.[11] For many such applications, the composition, morphology and thickness of the ultrathin cobalt oxide films (<10 nm) are crucial factors influencing their performance.[10–12]

Many methods have been developed for thin film fabrication, including spray pyrolysis, chemical vapor deposition (CVD), physical vapor deposition (PVD), pulse laser deposition (PLD), and atomic layer deposition (ALD).[14–20] Among these methods, ALD attracts great interest due to its self-limiting nature and exceptional coating conformality on three dimensional structures. While ALD generally exhibit a linear growth in the steady state, its growth behavior during the initial nucleation period could deviate considerably from the ideal layer-by-layer growth model, due to the complexity of nucleation and crystallinity of the deposited film.[21–24] While ALD growth of Co_3O_4 film on silicon-based substrates has been reported,[18,25,26] the ultrathin film characteristics during the initial growth stage has rarely reported in previous studies. Since the difference in the ultrathin film's thickness, composition, or morphology could lead to considerable changes in system properties,[27,28] it is thus of essential importance to understand the growth behavior of ALD grown cobalt oxide at the initial growth stage for the further optimization of CoO_x ultrathin films.

We report here a comprehensive study on the growth behavior of CoO_x ultrathin films (<10 nm) by ALD using $Co(Cp)_2$ and O_3 as precursors focusing on their composition and surface morphology. The coating conformality of CoO_x was evaluated on both planar and three dimensional substrates. At low deposition temperature of 150 °C, films are uniform and smooth, while island and uneven films are obtained after raising deposition temperature to 250 °C. The ultrathin film's composition is a mixture of CoO and Co_3O_4, which is different from its steady state counterpart in the bulk film. The obtained films show good CO oxidation catalytic performance which strongly correlates to the deposition temperature. Based on

[a]State Key Laboratory of Digital Manufacturing Equipment and Technology, School of Mechanical Science and Engineering, Huazhong University of Science and Technology, Wuhan 430074, People's Republic of China. E-mail: rongchen@mail.hust.edu.cn; Fax: +86-27-87558744; Tel: +86-27-87558744

[b]State Key Laboratory of Material Processing and Die and Mould Technology, School of Materials Science and Engineering, Huazhong University of Science and Technology, Wuhan 430074, People's Republic of China. E-mail: bshan@mail.hust.edu.cn

[c]School of Physics, Huazhong University of Science and Technology, Huazhong University of Science and Technology, Wuhan 430074, People's Republic of China

† Electronic supplementary information (ESI) available. See DOI: 10.1039/c5ra09782g

‡ These authors contributed equally to this work.

 This journal is © The Royal Society of Chemistry 2015

Published on 19 August 2015. Downloaded by Huazhong University of Science & Technology on 23/11/2015 02:29:49.

these observations, the growth behavior of ALD-CoO_x was discussed.

2. Experiments

CoO_x thin film was prepared by ALD in a commercial (SUNALE™ R200, Picosun) reactor. Thin film was grown on p-type silicon (100) as well as on nanoporous gold substrate. Cobaltocene (98%, $Co(Cp)_2$, Strem Chemicals) and ozone as precursors were supplied into the reactor in alternative cycles. High purity nitrogen (99.999%) was used as the sources carrier and purging gas. $Co(Cp)_2$ was held in a stainless steel bubbler maintained at 100 °C during deposition. O_3 was generated by feeding high purity O_2 (99.999%) into the ozone generator, which gives an O_3 volume concentration of ~11%. The deposition temperature was adjusted in the range from 100 °C to 300 °C. During the ALD deposition process, the chamber background pressure was controlled at 500 Pa. The entire ALD sequence consists 1.6 s pulse of $Co(Cp)_2$ and 2 s pulse of O_3 with 8 s purge of N_2 introduced in between. The flow rate of carrier gas for cobalt precursor and ozone was 50 sccm and 100 sccm, respectively.

The film thickness was measured by spectroscopic ellipsometer (SE, J. A. Woollam Co. M2000). The structure of thicker films was evaluated by Raman spectroscopy (LabRAM HR800) with 532 nm laser excitation. The chemical composition of ultrathin films was analyzed by X-ray photoelectron spectra (XPS, VG Multilab 2000) using a monochromatic Al Kα X-ray radiation. XPS data were fitted with XPSPEAK4.1 software and the binding energy was calibrated with respect of C 1s (284.6 eV) peak position. Surface morphology of freshly prepared samples was measured by a tapping mode atomic force microscopy (AFM, Agilent 5500) to avoid potential air-contacted contamination. Transmission electron microscope (TEM, JEOL-2010FEF) was operated with a 200 kV acceleration voltage to study the film morphology as well as crystallinity. To avoid the diffraction from substrate silicon and obtain stronger signals from ultrathin films, some samples were directly deposited on the TEM grid as well.

The catalytic activity toward oxidation of CO was tested in a home-built stainless reactor. All samples were deposited on Si wafer with area of 1 cm*2 cm at different deposition temperature. For the evaluation of catalytic activity, the flow rate of inlet gas is set to 5 sccm controlled through a mass flow controller (Sevenstar, Beijing Sevenstar Electronics Co., Ltd), containing 1% CO, 10% O_2 diluted in argon gas. Temperature is raised up from room temperature to 310 °C with a ramped rate of approx. 2 °C min^{-1}. Data was recorded with a thermocouple attached at the bottom of the samples. A quadrupole mass spectrometers (QMS) was connected to the outlet to monitor the exhaust gas. All these setup of this planar catalyst system gives high sensitivity and reproducibility for CO conversion.

3. Results

3.1. ALD deposition parameters

Cobalt oxide films were prepared with deposition temperatures in the range of 100–300 °C. The film's thickness and growth rate were monitored as functions of deposition temperature. Fig. 1(a) illustrates the dependence of growth per cycle (GPC) as a function of deposition temperature. The growth rate is relatively slow when the deposition temperature is below 150 °C, due to the lack of thermal activation energy. Then it reaches a steady growth rate of 0.37 Å per cycle in the temperature range from 150 °C to 250 °C, consistent with previous literatures.[18] The growth rate increases abruptly when the temperature goes beyond 250 °C, partially due to the thermal decomposition of precursors. According to the data, stable ALD temperature window was determined between 150 °C and 250 °C.

The film's thickness as a function of deposition cycles was plotted in Fig. 1(b). Ideally linear growth as a function of ALD cycles is shown at low deposition temperature (150 °C). However, films deposited at 250 °C show inhibited growth in the initial cycles as indicated by the thinner film thickness and nonlinear growth curve for the first 100 cycles. This phenomenon implies a relative slow nucleation rate at 250 °C as evidence by the slower growth rate in the initial 100 cycles.

3.2. Composition of ultrathin films

In terms of film composition, previous XRD study indicates that Co_3O_4 is the major component for bulk film deposited by ALD while CoO only forms at deposition temperature higher than 331 °C.[18] In our study, Raman spectra were first explored to survey thick (~100 nm) samples (Fig. 2). The A_{1g}, E_g and three T_{2g} modes are Raman active for the spinel structure Co_3O_4 with Co^{2+} and Co^{3+} located at tetrahedral and octahedral site, respectively.[29,30] Raman spectra indicate that the main composition of our thick CoO_x samples primarily consists of Co_3O_4.

However, the situation is considerably different when ultrathin CoO_x film is deposited. X-ray photoelectron spectroscopy (XPS), a surface sensitive analytical technique, was conducted to investigate the film's composition at the initial growth stage with different film thickness and deposition temperature. High resolution Co 2p spectra shown in Fig. 3(a) and (b) splits into two peaks, which can be attributed to Co $2p_{1/2}$ and Co $2p_{3/2}$. No metallic cobalt impurity exists in the film since there is no peak at the binding energy (E_b) for metallic cobalt located at ~778 eV.[31] For films deposited at 150 °C with thickness larger than 6 nm, the Co binding energy (E_b(Co $2p_{3/2}$) is located at ~780 eV and E_b(Co $2p_{1/2}$) at ~795 eV) is in a good agreement with that of Co_3O_4.[31–34] However, when the film is thin enough (for example, thickness $\leq$ 1 nm), the binding energy for main Co $2p_{3/2}$ and Co $2p_{1/2}$ shifts to ~780.4 eV and ~796.1 eV, which corresponds to the signatures of CoO.[31,35] What's more, the satellite peak located at 5.6 eV higher than the main peak gradually appears. This is strong evidence for the existence of CoO at the initial grown stage, and the film composition gradually changes to Co_3O_4 for the steady growth.[10,31–33,35–38] The composition evolution of film deposited at 250 °C shows a similar trend. The satellite peak disappears gradually with the increase of the film thickness. The only noticeable difference from that of 150 °C is the relatively slower conversion speed, thus thicker films are required to show such transition behavior (Fig. 3(b)). The O 1s XPS spectrum is given in Fig. 3(c) and (d).

Published on 19 August 2015. Downloaded by Huazhong University of Science & Technology on 23/11/2015 02:29:49.

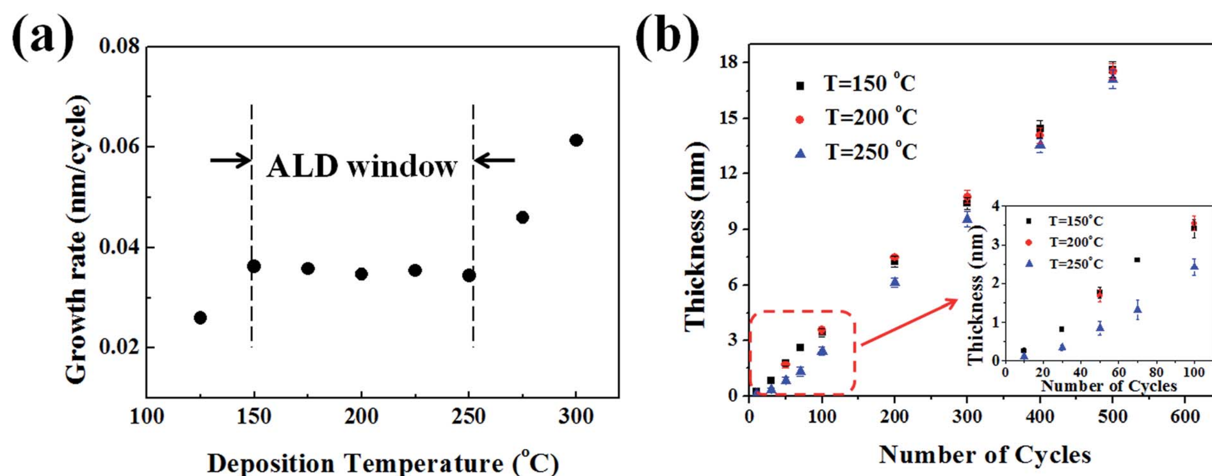

Fig. 1 (a) The growth rate of cobalt oxide as a function of deposition temperature, (b) dependence of film thickness on the number of ALD cycles at different temperature.

The peak located at ∼531.5 eV can be attributed to near surface chemisorbed oxygen species to oxygen vacancies (OH^-, O^{2-} *et al.*), which is indicative of cobalt oxide surface[39,40] and was not from surface contaminations. This peak could be observed at initial growth stage of cobalt oxide deposited at both 150 °C and 250 °C. The peak locates at ∼529.5 eV can be ascribed to lattice oxygen of Co_3O_4.[41] When the thickness reaches a turning point, film composition gradually becomes pure Co_3O_4 which may leads to the peak appearance at 529.5 eV. Compared with deposition done at 250 °C, this peak for lattice oxygen of Co_3O_4 was observed for thinner film at deposition temperature of 150 °C. The phenomenon indicates a quicker composition transformation at lower deposition temperature. Our results show that the composition is the mixture of Co_3O_4 and CoO for ultrathin CoO_x film, and the content of Co_3O_4 phase increases with the increase of ALD cycles. After a threshold of ALD cycles the CoO ratio would fall below the detection limit and the whole film appear to be pure Co_3O_4. The speed of the conversion is faster at lower deposition temperature. Our Raman and XPS results reveal that CoO forms during the initial growth stage within the ALD temperature window, while the subsequent layer by layer growth results in Co_3O_4 films.

3.3. Surface morphology and crystallinity of ultrathin films

The surface morphology of ultrathin cobalt oxide films were monitored by AFM. To guarantee the accuracy of AFM analysis, Si substrate was treated in vacuum condition at elevated temperatures of 150 °C, 200 °C and 250 °C. From AFM tests (Fig. S3†), the surface morphology and roughness (RMS 0.3–0.4 nm) of Si wafer after such treatment were stable and thus the substrate effect in the following AFM analysis could be ruled out. Fig. 4 shows the film's surface morphology as the function of ALD cycles and substrate temperatures. For films grown at 150 °C, the silicon surface was fully occupied by continuous cobalt oxide film after 100 ALD cycles. The surface appears smooth and continuous, and does not change much with the increase of ALD cycles. The film's microstructure changes significantly after raising the deposition temperature. Surface of the film becomes rough and porous when grown at 200 °C. For the 250 °C deposition, discontinuous film is obtained with a wide distribution of grain size and a relatively low islands density. The existence of large particles is often related to the crystalline film growth.[10,31–33,35–38]

Fig. 5 shows the data for the dependence of film's RMS evolution on deposition temperature and growth cycles. The film's roughness keeps about the same at 150 °C with the increase of ALD cycles. As a comparison, roughness of films grown at 250 °C is much larger and keeps increasing at the initial 300 cycles. The RMS for 400 cycles cobalt oxide at 250 °C is lower than 300 cycles film, due to the merging of neighboring grains. This result shows a strong relationship between the deposition parameters and the resulting feature of the ultrathin cobalt oxide film.

To study the crystallinity of ALD ultrathin cobalt oxide, films were directly deposited on the TEM grid to avoid the signals from silicon substrate and obtain stronger diffractions from

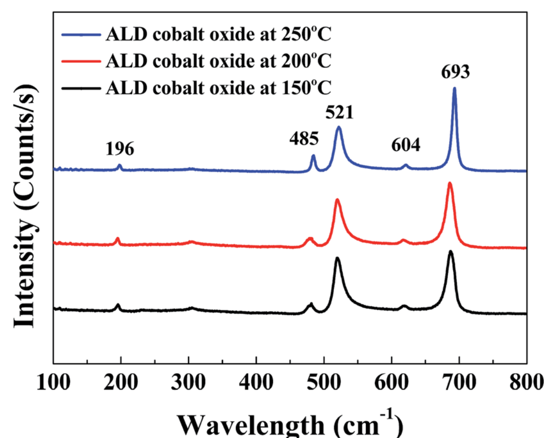

Fig. 2 Raman spectra for thick samples deposited at 150 °C, 200 °C and 250 °C.

 This journal is © The Royal Society of Chemistry 2015

Published on 19 August 2015. Downloaded by Huazhong University of Science & Technology on 23/11/2015 02:29:49.

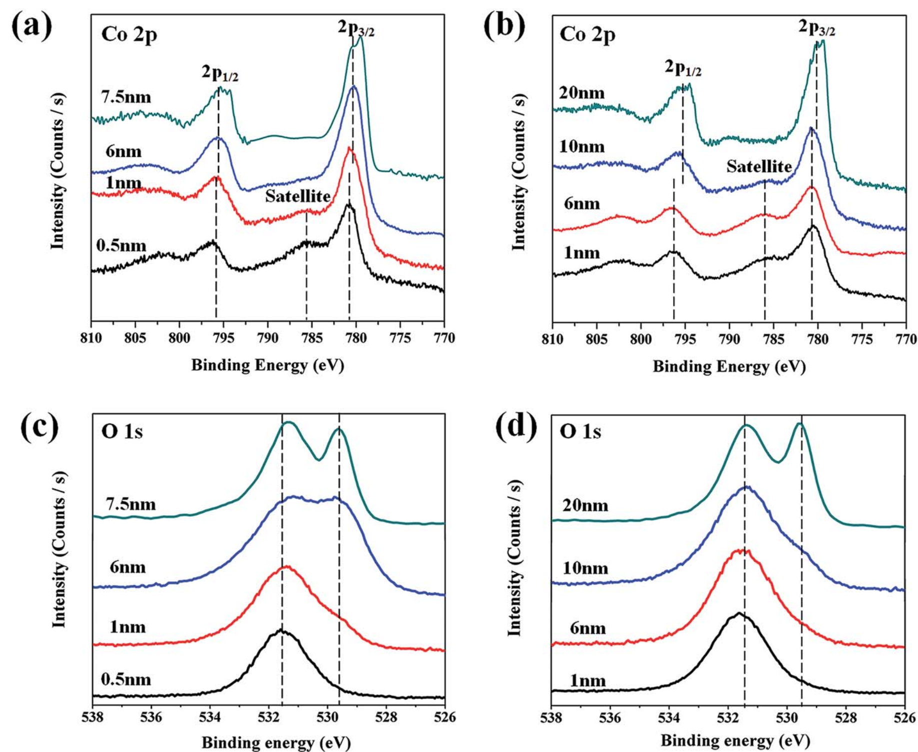

Fig. 3 XPS spectra evolution for (a) Co 2p at 150 °C, (b) Co 2p at 250 °C, (c) O 1s at 150 °C and (d) O 1s at 250 °C.

ultrathin films. Fig. 6 shows the TEM images and diffraction patterns for samples after 100, 200 and 300 ALD cycles. The difference of films' feature is consistent with the AFM observation that low density of islands and large crystal size were observed at 250 °C. Besides, the particles tend to crystallize more easily at 250 °C than that at 150 °C as indicated by the selected area electron diffraction (SAED) patterns (Fig. 6, inset). From the SAED patterns, cobalt oxide synthesis at 250 °C have

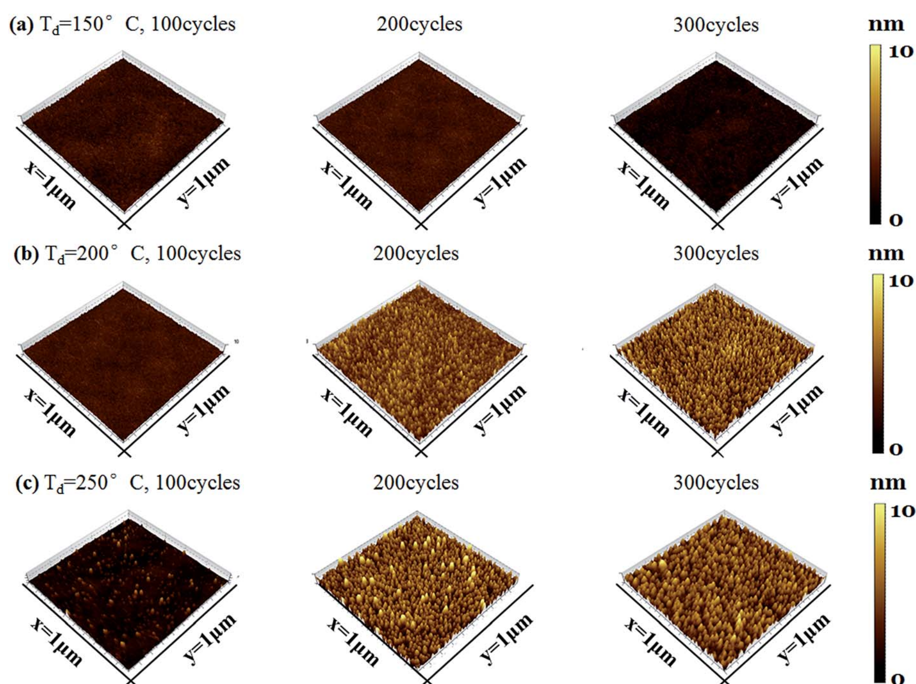

Fig. 4 Surface morphology evolution for cobalt oxide deposited at (a) 150 °C, (b) 200 °C and (c) 250 °C for 100, 200 and 300 cycles.

Published on 19 August 2015. Downloaded by Huazhong University of Science & Technology on 23/11/2015 02:29:49.

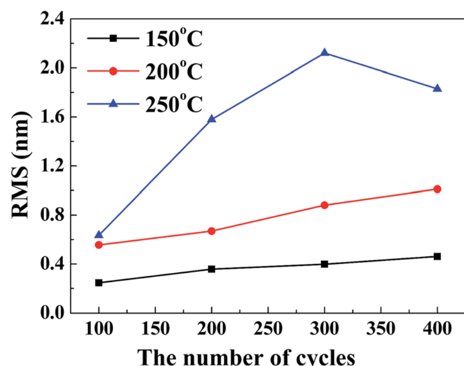

Fig. 5 RMS evolution as the function of deposition temperature and ALD cycles.

crystalline structure from initial 100 cycles while cobalt oxide synthesis at 150 °C is amorphous. As ALD cycles increase, both samples have preferred crystalline orientation of (220), (311) and (331) as three nearest lattice planes.

3.4. Coating conformality on three dimensional substrates

The aforementioned growth behavior of CoO_x ultrathin film applies not only on planar substrates, but also on three dimensional high surface area structures. In addition to silicon substrate, cobalt oxide was coated on nanoporous gold substrate to investigate the oxide layer's morphology and coating conformality. The deposition recipe was the same as films grown on planer substrate. TEM was employed for samples covered by 100 cycles ALD cobalt oxide at 150 °C and 250 °C. Result presented in Fig. 7(a) shows very good coating conformality and ultra-smooth surface for films grown at 150 °C. Detailed analysis by TEM illustrated in Fig. S1† shows that the film is already continuous only after 50 cycles with the thickness less than 2 nm. In contrast, cobalt oxide deposited at 250 °C shows individual islands. With the increase of ALD cycles, the islands grow and merge with their neighbors gradually. This observation is consistent with the results found by AFM where the surface roughness is dependent on deposition temperature. In addition, HR-TEM observation also reveals that films are easy to be crystalline at high deposition temperature.

Side view HRTEM characterization for cobalt oxide grown on porous gold at both 150 °C and 250 °C with increasing ALD

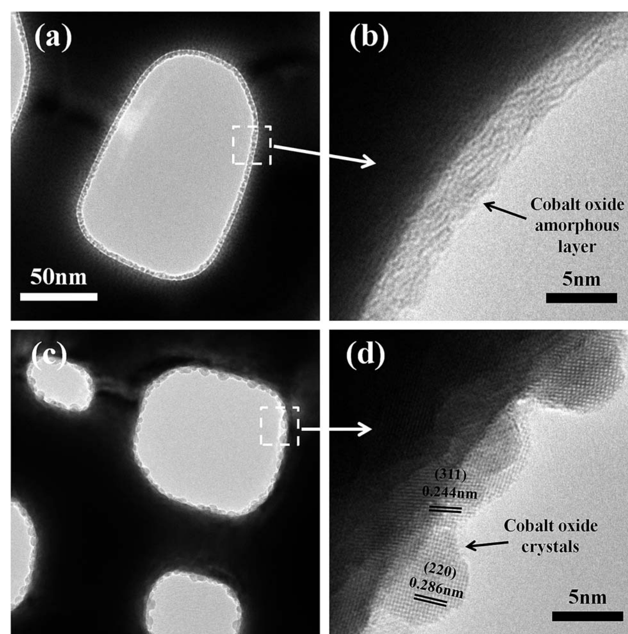

Fig. 7 TEM observation for nanoporous gold samples coated by 100 cycles ALD cobalt oxide at (a), (b) 150 °C and (c and d) 250 °C.

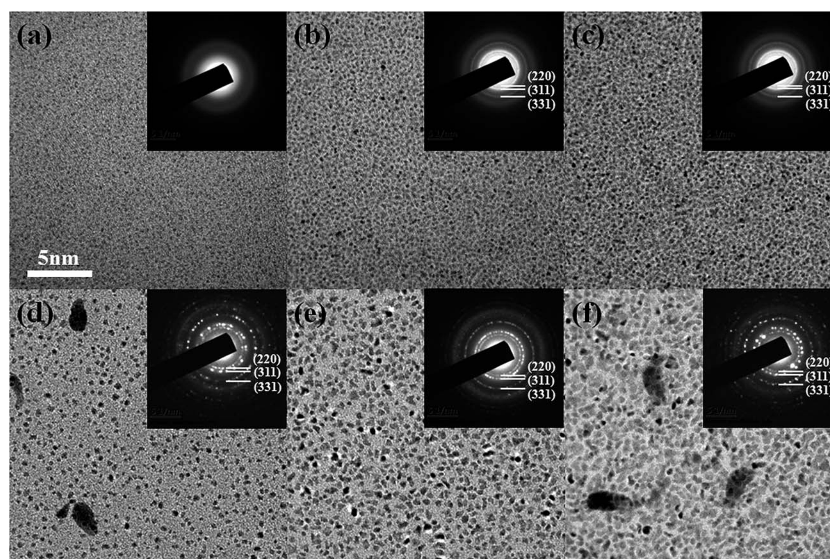

Fig. 6 TEM images and diffraction patterns of cobalt oxide grown for (a and d) 100 cycles, (b and e) 200 cycles and (c and f) 300 cycles at (a–c) 150 °C and (d–f) 250 °C.

This journal is © The Royal Society of Chemistry 2015

Published on 19 August 2015. Downloaded by Huazhong University of Science & Technology on 23/11/2015 02:29:49.

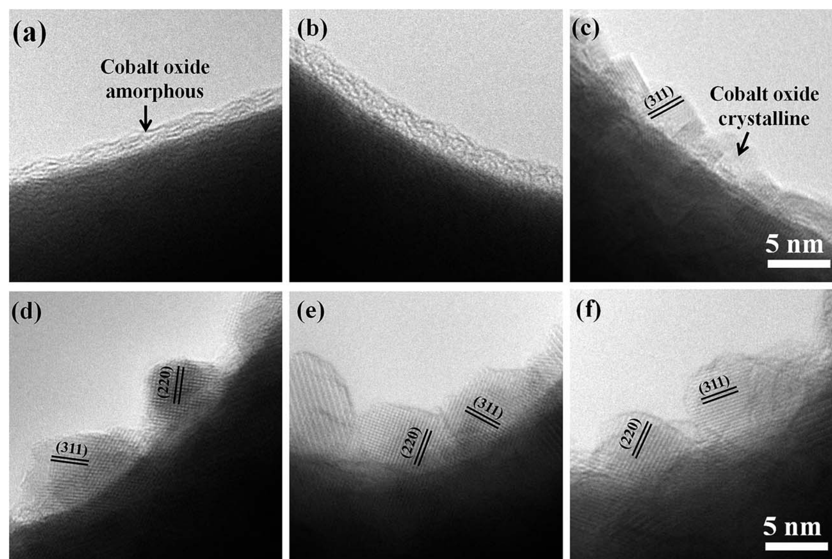

Fig. 8 HRTEM images cobalt oxide deposited on nanoporous gold with 50, 100, 200 cycles ALD at (a–c) 150 °C and (d–e) 250 °C respectively.

cycles are shown in Fig. 8. From HRTEM images, it can be seen that deposited cobalt oxide is amorphous in the initial stage at 150 °C, and change into crystalline structure as ALD cycles increase. At 250 °C, crystalline structure was observed in the initial stage which is consistent as SAED pattern indicate. (311) and (220) directions are preferred growth orientations for both deposition temperature.

4. Discussions

Two different growth modes exist for ultrathin ALD-CoO_x films on both planar and three dimensional structures. Both growth temperature and film thickness strongly affect its morphology and crystallinity. Combining with the observation of initial growth curve, AFM, and TEM, the factors dominate the ultra-thin cobalt oxide growth modes can be ascribed to the number of nucleation site density and the speed of crystallization.

With regard to the nucleation site density, the chemisorption of the precursors on the surface of the substrate is the dominant factor in the initial nucleation process. The nucleation events generally occur more easily on the surface active sites (defects or surface function groups). As indicated by the initial growth curve (Fig. 1(b)), AFM and TEM observations, the cobalt oxide shows poor nucleation under 250 °C. Literatures indicated that the density of surface hydroxyl group on silicon substrate was temperature-dependent and decreases at higher temperatures due to the dehydroxylation process.[42–46] Since the loss of surface hydroxyl would retard the nucleation process, it is reasonable that cobalt oxide film shows poorer nucleation, longer incubation cycles, and lower density of grown islands at 250 °C. The same conclusion holds on nanoporous gold substrate. The surface of nanoporous gold was reported to have strong ability for the adsorption of molecular water, resulting in the formation of hydroxyl species on the gold surface.[47–49] The concentration of adsorbed hydroxyl species on the gold surface would also decrease with rising deposition temperature.[50,51] Therefore, the nucleation sites of cobalt oxide grown on porous gold at 250 °C are limited due to the reduction of hydroxyl group, inducing the lower density of nuclei. The effect of surface hydroxyl groups on the film growth has been further confirmed by CoO_x deposition experiment on piranha treated Si samples (Fig. S2†).

With regard to the film crystallinity, the deposition temperature also plays a crucial role. The trend of crystallinity as function of temperature has been observed in the previous study of ALD metal oxide (TiO_2, HfO_2, ZrO_2) that high temperature can promote the surface mobility of the absorbed species and enhance the ordering of the structure with more energy available for crystallization.[46,52–54] Therefore, films deposited at relatively high temperatures normally include more crystalline phase. The crystallites occur more easily at higher temperatures inducing the very fast crystal growth along specific orientations (in our case, (220) and (311) for cobalt oxide growth).[44,46] On the other hand, lower nucleation density decreases the steric hindrance on adsorption of precursors. Therefore, the precursors can easily adsorb on the boundary of the islands and promote the growth of the individual oxide particles rapidly, leading to the rough surface formation. The AFM (Fig. 4) and TEM (Fig. 6) observation confirms the growth and crystallization of the large islands. As discussed above, the relatively small number of nucleation sites and the fast crystallization speed function coherently and cause the rough and discontinuous CoO_x film morphology at 250 °C.

Finally, CO oxidation activity was studied to illustrate the effect of deposition parameters on its catalytic activity. Samples were deposited at 150 °C, 200 °C and 250 °C (designated as $T_{150\ °C}$, $T_{200\ °C}$ and $T_{250\ °C}$) with thickness of ~10 nm. Bare Si wafer with the same area was used for comparison. Obviously, all cobalt oxide films show negative temperature shift relative to bare Si wafer (see Fig. 9). A noticeable tendency can be observed

Published on 19 August 2015. Downloaded by Huazhong University of Science & Technology on 23/11/2015 02:29:49.

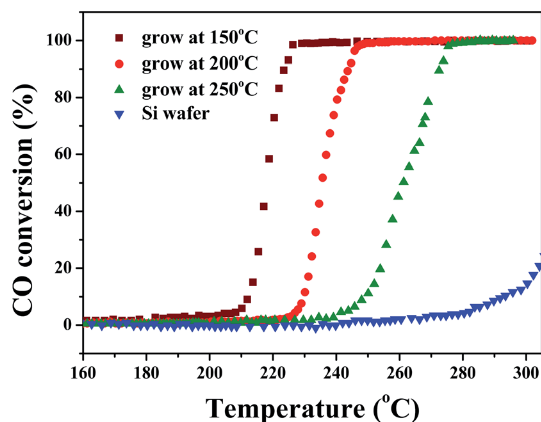

Fig. 9 CO oxidation light off test of cobalt oxide thin film catalyst grown under different temperature.

that the catalytic ability is in the following order: $T_{150\ °C} > T_{200\ °C} > T_{250\ °C}$. This result is reasonable since it is generally accepted that the oxidation of CO is attributed to the existence of Co^{3+} cation. The CO can be more easily absorbed on the Co^{3+} sites and react with the oxygen to form CO_2.[50,51] Thus, higher content of Co_3O_4 would in general lead to better CO oxidation catalytic activity. For cobalt oxide films deposited at lower temperatures, the composition is primarily Co_3O_4, while there still exists a larger portion of CoO in the film deposited at higher temperatures. Controlled experiments were further carried out to determine the influence of composition and morphology to the catalyst activity (detail results are given in ESI, Fig. S4–6†), which reveals that surface oxygen and cobalt oxide composition are two main factors influencing the catalytic performance. Those results confirm the importance for composition control of ALD CoO_x ultrathin film.

5. Conclusions

In this work, we systematically studied the composition, morphology and crystallinity of ultrathin cobalt oxide film grown by ALD using $Co(Cp)_2$ and O_3 on both planar and three dimensional substrate. In the ALD temperature window (150–250 °C), mixture of Co_3O_4 and CoO forms at the initial growth stage. Compared with the smooth and continuous film obtained at 150 °C, films roughness increases with the formation of large and individual particles at high deposition temperature (250 °C). We reveal that the initial growth behavior is primarily related to the number of nucleation sites and the speed of crystallization. Films deposited with different deposition temperatures show distinctive differences in catalytic activity towards CO oxidation. Our detailed study gains insight into initial CoO_x film's ALD growth and could be utilized to further manipulate its morphology and composition for various applications.

Acknowledgements

The authors would like to acknowledge equipment supports from AMETEK lab and the technology support by the Analytic Testing Center of HUST. This work is supported by the National Basic Research Program of China (2013CB934800), the National Natural Science Foundation of China (51575217 and 51572097), the Fundamental Research Funds for the Central Universities, HUST (2014TS037) and the Hubei Province Funds for Distinguished Young Scientists (2014CFA018, 2015CFA034). Rong Chen acknowledges the Thousand Young Talents Plan, the Recruitment Program of Global Experts, and Program for Changjiang Scholars and Innovative Research Team in University (No. IRT13017).

References

1 E. C. Tyo, C. R. Yin, M. Di Vece, Q. Qian, G. Kwon, S. Lee, B. Lee, J. E. DeBartolo, S. Seifert, R. E. Winans, R. Si, B. Ricks, S. Goergen, M. Rutter, B. Zugic, M. Flytzani-Stephanopoulos, Z. W. Wang, R. E. Palmer, M. Neurock and S. Vajda, *ACS Catal.*, 2012, **2**, 2409–2423.
2 N. Fontaíña-Troitiño, S. Liébana-Viñas, B. Rodríguez-González, Z.-A. Li, M. Spasova, M. Farle and V. Salgueiriño, *Nano Lett.*, 2014, **14**, 640–647.
3 A. U. Mane and S. A. Shivashankar, *J. Cryst. Growth*, 2003, **254**, 368–377.
4 S. G. Kandalkar, J. L. Gunjakar and C. D. Lokhande, *Appl. Surf. Sci.*, 2008, **254**, 5540–5544.
5 M. E. Donders, H. C. M. Knoops, W. M. M. Kessels and P. H. L. Notten, *J. Power Sources*, 2012, **203**, 72–77.
6 X. Xie, Y. Li, Z.-Q. Liu, M. Haruta and W. Shen, *Nature*, 2009, **458**, 746–749.
7 A. Alvarez, S. Ivanova, M. A. Centeno and J. A. Odriozola, *Appl. Catal., A*, 2012, **431–432**, 9–17.
8 M. J. Pollard, B. A. Weinstock, T. E. Bitterwolf, P. R. Griffiths, A. Piers Newbery and J. B. Paine Iii, *J. Catal.*, 2008, **254**, 218–225.
9 L. Xi, P. D. Tran, S. Y. Chiam, P. S. Bassi, W. F. Mak, H. K. Mulmudi, S. K. Batabyal, J. Barber, J. S. C. Loo and L. H. Wong, *J. Phys. Chem. C*, 2012, **116**, 13884–13889.
10 S. C. Riha, B. M. Klahr, E. C. Tyo, S. Seifert, S. Vajda, M. J. Pellin, T. W. Hamann and A. B. F. Martinson, *ACS Nano*, 2013, **7**, 2396–2405.
11 M. F. Lichterman, M. R. Shaner, S. G. Handler, B. S. Brunschwig, H. B. Gray, N. S. Lewis and J. M. Spurgeon, *J. Phys. Chem. Lett.*, 2013, **4**, 4188–4191.
12 B. Huang, W. Yang, Y. Wen, B. Shan and R. Chen, *ACS Appl. Mater. Interfaces*, 2015, **7**, 422–431.
13 L. Trotochaud, T. J. Mills and S. W. Boettcher, *J. Phys. Chem. Lett.*, 2013, **4**, 931–935.
14 V. R. Shinde, S. B. Mahadik, T. P. Gujar and C. D. Lokhande, *Appl. Surf. Sci.*, 2006, **252**, 7487–7492.
15 J. Tyczkowski, R. Kapica and J. Łojewska, *Thin Solid Films*, 2007, **515**, 6590–6595.
16 N. Bahlawane, E. Fischer Rivera, K. Kohse-Höinghaus, A. Brechling and U. Kleineberg, *Appl. Catal., B*, 2004, **53**, 245–255.
17 T. Warang, N. Patel, A. Santini, N. Bazzanella, A. Kale and A. Miotello, *Appl. Catal., A*, 2012, **423–424**, 21–27.

This journal is © The Royal Society of Chemistry 2015

Published on 19 August 2015. Downloaded by Huazhong University of Science & Technology on 23/11/2015 02:29:49.

18 M. Diskus, O. Nilsen and H. Fjellvåg, *Chem. Vap. Deposition*, 2011, **17**, 135–140.
19 B. Han, K. H. Choi, K. Park, W. S. Han and W.-J. Lee, *Electrochem. Solid-State Lett.*, 2011, **15**, D14–D17.
20 R. Edla, N. Patel, Z. El Koura, R. Fernandes, N. Bazzanella and A. Miotello, *Appl. Surf. Sci.*, 2014, **302**, 105–108.
21 S. Novak, B. Lee, X. Yang and V. Misra, *J. Electrochem. Soc.*, 2010, **157**, H589–H592.
22 L. Baker, A. S. Cavanagh, D. Seghete, S. M. George, A. J. M. Mackus, W. M. M. Kessels, Z. Y. Liu and F. T. Wagner, *J. Appl. Phys.*, 2011, **109**, 084333–084310.
23 A. Tamm, M. C. Dimri, J. Kozlova, A. Aidla, T. Tätte, T. Arroval, U. Mäeorg, H. Mändar, R. Stern and K. Kukli, *J. Cryst. Growth*, 2012, **343**, 21–27.
24 R. L. Puurunen and W. Vandervorst, *J. Appl. Phys.*, 2004, **96**, 7686–7695.
25 M. Rooth, E. Lindahl and A. Hårsta, *Chem. Vap. Deposition*, 2006, **12**, 209–213.
26 K. B. Klepper, O. Nilsen and H. Fjellvåg, *Thin Solid Films*, 2007, **515**, 7772–7781.
27 J. Luo, S. K. Karuturi, L. Liu, L. T. Su, A. I. Y. Tok and H. J. Fan, *Sci. Rep.*, 2012, **2**, 451.
28 L. Qian, W. Shen, B. Shen, G. W. Qin and B. Das, *Nanotechnology*, 2010, **21**, 305705.
29 N. Bahlawane, P. H. T. Ngamou, V. Vannier, T. Kottke, J. Heberle and K. Kohse-Hoinghaus, *Phys. Chem. Chem. Phys.*, 2009, **11**, 9224–9232.
30 C.-W. Tang, C.-B. Wang and S.-H. Chien, *Thermochim. Acta*, 2008, **473**, 68–73.
31 M. C. Biesinger, B. P. Payne, A. P. Grosvenor, L. W. M. Lau, A. R. Gerson and R. S. C. Smart, *Appl. Surf. Sci.*, 2011, **257**, 2717–2730.
32 D. Barreca, C. Massignan, S. Daolio, M. Fabrizio, C. Piccirillo, L. Armelao and E. Tondello, *Chem. Mater.*, 2001, **13**, 588–593.
33 S. C. Petitto, E. M. Marsh, G. A. Carson and M. A. Langell, *J. Mol. Catal. A: Chem.*, 2008, **281**, 49–58.
34 S. Pasko, A. Abrutis, L. G. Hubert-Pfalzgraf and V. Kubilius, *J. Cryst. Growth*, 2004, **262**, 653–657.
35 S. Wang, B. Zhang, C. Zhao, S. Li, M. Zhang and L. Yan, *Appl. Surf. Sci.*, 2011, **257**, 3358–3362.
36 M. Voß, D. Borgmann and G. Wedler, *J. Catal.*, 2002, **212**, 10–21.
37 T. Q. Ngo, A. Posadas, H. Seo, S. Hoang, M. D. McDaniel, D. Utess, D. H. Triyoso, C. B. Mullins, A. A. Demkov and J. G. Ekerdt, *J. Appl. Phys.*, 2013, **114**, 084901–084908.
38 M. Burriel, G. Garcia, J. Santiso, A. Abrutis, Z. Saltyte and A. Figueras, *Chem. Vap. Deposition*, 2005, **11**, 106–111.
39 D. Ledue, A. Maitre, F. Barbe and L. Lechevallier, *J. Magn. Magn. Mater.*, 2014, **372**, 134–140.
40 S. C. Petitto, E. M. Marsh, G. A. Carson and M. A. Langell, *J. Mol. Catal. A: Chem.*, 2008, **281**, 49–58.
41 M. Konsolakis, M. Sgourakis and S. A. C. Carabineiro, *Appl. Surf. Sci.*, 2015, **341**, 48–54.
42 R. Matero, A. Rahtu, M. Ritala, M. Leskelä and T. Sajavaara, *Thin Solid Films*, 2000, **368**, 1–7.
43 A. Dkhissi, G. Mazaleyrat, A. Esteve and M. D. Rouhani, *Phys. Chem. Chem. Phys.*, 2009, **11**, 3701–3709.
44 M. Cassir, F. Goubin, C. Bernay, P. Vernoux and D. Lincot, *Appl. Surf. Sci.*, 2002, **193**, 120–128.
45 G. Scarel, S. Ferrari, S. Spiga, C. Wiemer, G. Tallarida and M. Fanciulli, *J. Vac. Sci. Technol., A*, 2003, **21**, 1359–1365.
46 D. M. Hausmann and R. G. Gordon, *J. Cryst. Growth*, 2003, **249**, 251–261.
47 X. Ge, R. Wang, P. Liu and Y. Ding, *Chem. Mater.*, 2007, **19**, 5827–5829.
48 G. Mullen, J. Gong, T. Yan, M. Pan and C. B. Mullins, *Top. Catal.*, 2013, **56**, 1499–1511.
49 C. L. Platt, N. Li, K. Li and T. M. Klein, *Thin Solid Films*, 2010, **518**, 4081–4086.
50 C. K. Costello, J. H. Yang, H. Y. Law, Y. Wang, J. N. Lin, L. D. Marks, M. C. Kung and H. H. Kung, *Appl. Catal., A*, 2003, **243**, 15–24.
51 C. K. Costello, M. C. Kung, H. S. Oh, Y. Wang and H. H. Kung, *Appl. Catal., A*, 2002, **232**, 159–168.
52 J. Aarik, A. Aidla, T. Uustare and V. Sammelselg, *J. Cryst. Growth*, 1995, **148**, 268–275.
53 M. Ritala, M. Leskelä, L. Niinistö, T. Prohaska, G. Friedbacher and M. Grasserbauer, *Thin Solid Films*, 1994, **250**, 72–80.
54 J. Liu, X. B. Meng, M. N. Banis, M. Cai, R. Y. Li and X. L. Sun, *J. Phys. Chem. C*, 2012, **116**, 14656–14664.